



Design of Sievert Type Apparatus: Cooling Mode Heat Transfer Analysis in Hydrogen Sievert Apparatus

Hifni Mukhtar Ariyadi^{1,2}, Robertus Dhimas Dewangga Putra^{1,2,*},
Burhan Febrinawarta^{1,2}, Agung Nugroho³, Hanida Nilasary⁴, and
Haryo Satriya Oktaviano⁴

¹ Department of Mechanical and Industrial Engineering, Faculty of Engineering,
Universitas Gadjah Mada, Jl. Grafika No. 2 Yogyakarta, 55281 Indonesia

² Centre for Energy Studies, Universitas Gadjah Mada, Sekip Blok K1-A
Yogyakarta 55281 Indonesia

³ Department of Chemical Engineering, Universitas Pertamina, Jalan Teuku Nyak Arief,
Simprug Kebayoran Lama, Jakarta 12220, Indonesia

⁴ Downstream Research and Technology Innovation, Research and Technology Innovation, PT
Pertamina (Persero), Sopo Del Tower A Floor 51, Jakarta 12950, Indonesia

Corresponding Author's email: robertus.dhimas.d.p@ugm.ac.id

Abstract. Porous carbon is one alternatives material to store hydrogen through adsorption mode known as solid state hydrogen storage (SSHS). The capacity of this SSHS could be analyzed using volumetric technique, measuring the changing of pressure at known volume and temperature. The measurement equipment using this technique is known as sievert type apparatus. In this work heat transfer analysis was conducted during the design of sievert type apparatus to ensure no gradient temperature or could spot in the apparatus as well as to analyze the time vs cooler flow rate for the targeted measurement temperature. Two analyses were carried out using analytical lumped capacitance method and numerical computational fluid dynamics (CFD). The findings indicate that increasing the mass flow rate from 0.01 kg/s to 0.25 kg/s leads to a substantial reduction in cooling time, decreasing it from 3250 seconds to 250 seconds. However, further increasing the mass flow rate beyond 0.25 kg/s does not significantly decrease the cooling time. The maximum heat transfer rate is 700 W and achieving the target temperature with a coolant flow rate of 50 g/s takes only 380 seconds when using a numerical approach with CFD, which is faster than the analytical results.

Keywords: Sievert Type Apparatus, CFD, SSHS, Analytical lumped capacitance method, Poros carbon.

1 INTRODUCTION

The global energy landscape is undergoing a profound transformation, driven by increasing concerns over climate change, the pursuit of cleaner energy sources, and a growing demand for energy across the world. As traditional fossil fuels face scrutiny due to their environmental impact, the need for clean and sustainable alternatives has never been more critical. Hydrogen is a versatile energy source that can be combusted to produce heat (without emitting carbon) or used in conjunction with fuel cells to

© The Author(s) 2025

M. A. Muflikhun et al. (eds.), *Proceedings of the 10th International Conference on Science and Technology (ICST 2024)*, Advances in Engineering Research 268,

https://doi.org/10.2991/978-94-6463-772-4_58

produce current. It has the highest energy density (142 MJ/kg) among other energy sources such as gasoline (45.8 MJ/kg), methane (47.2 MJ/kg), or Lithium battery (0.9-2.49 MJ/kg). However, storing hydrogen in an economical way is not a simple task [1], [2]. To be economically feasible hydrogen should be stored under the pressure of 700 bar in the gas phase or cryogenically cooled below 20 K in the liquid phase. The process of compression and liquefaction would raise concerns in both safety and energy required for the processes. Solid-state hydrogen storage (SSHS) can be a promising alternative to storing hydrogen in terms of economical and safety [3].

Hydrogen storage in solid form can be achieved through both adsorption and absorption processes. In both processes, there are criteria such as gravimetric (2.6 w.t.% H₂) and volumetric energy density (1.7 kg H₂/L) for material be feasible for SSHS [4]. Carbon-based material or activated carbon is a promising material for SSHS, through adsorption process, with a capacity of up to 5.7 wt% or 1.9 kWh/kg, knowing the energy density of hydrogen is 33.3 kWh/kg [5]. This energy density is substantially higher than commercial lithium-polymer batteries which have the energy density of 200-250 Wh/kg. In addition, carbon-based materials are known to have higher hydrogen storage capacity at low temperatures [6].

To ensure the feasibility of carbon-based materials for SSHS, the measurement of hydrogen capacity is an important step subsequent the synthesis of material. The hydrogen adsorption capacity of a SSHS material can be conducted by volumetric technique. This technique is essentially analyzing the changing of pressure with knowing volume and temperature [7]. The measurement apparatus using this volumetric technique is known as Sievert Type Apparatus (STA).

One of the challenges in hydrogen capacity measurement of carbon based SSHS is the requirement of low temperature measurement subsequent to volume calibration using helium at high temperature [8]. The highest gradient of measurement temperature to the ambient temperature might result in the greater error during isothermal measurement [9]. In some cases, parts of the measurement apparatus have lower temperature than the rest, known as cold spot, and lead to error during volumetric measurements [10]. During the measurement, the temperature in the whole chamber must be maintained uniform and thus the analysis of heat transfer is very essential during the STA design process.

This paper presents heat transfer analysis on the cooling process during hydrogen adsorption on carbon based SSHS. The analysis is conducted in two different methods, analytically using lumped capacitance method, and numerically using computational fluid dynamics (CFD). The primary goal of this research is to enhance our understanding of the heat transfer dynamics during the cooling phase of hydrogen adsorption on carbon-based SSHS. The results will be beneficial for designing, optimizing, and improving the efficiency of SSHS systems, which have applications in hydrogen storage for various clean energy technologies. By comparing the results of analytical and numerical methods, the research aims to provide a comprehensive and validated analysis of the heat transfer in this specific process, contributing to the broader goal of advancing hydrogen storage technologies and promoting sustainable and clean energy solutions.

2 METHODOLOGY

The heat transfer analysis for the cooling process of hydrogen in the chamber are conducted using both the lumped analysis approach and computational fluid dynamics (CFD) simulations.

2.1 Lumped Capacitance Analysis

The lumped capacitance method is a technique used to simplify the analysis of heat transfer in a system by disregarding internal temperature variations within an object or system. This method is applicable to objects with specific geometries and properties that allow this assumption to be made without significant loss of accuracy.

In a system with lumped capacitance conditions, the object or system, i.e. Sievert reactor, is assumed to possess characteristics referred to as "lumped" or "centralized," meaning that the temperature of the object or system is considered to be uniform throughout its entire volume at a given time. This assumption typically applies to objects with high thermal conductivity and relatively small geometrical sizes.

Calculations using the lumped capacitance method can be performed by using Eq. (1)

$$\frac{\theta}{\theta_i} = \frac{T - T_\infty}{T_i - T_\infty} = \exp \exp \left[- \left(\frac{h A_s}{\rho V c} \right) t \right] \quad (1)$$

In Eq. (1), T is the average temperature of the object (hydrogen and Sievert reactor) at time t (K), T_∞ is the temperature of the cooling fluid (K), T_i is the initial temperature of the object (hydrogen and chamber) at time $t = 0$ (K), h is the convective heat transfer coefficient from the object to the cooling fluid ($\text{W}/\text{m}^2 \cdot \text{K}$), A_s is the surface area of the object (m^2), ρ is the density of the object (kg/m^3), V is the volume of the object (m^3), c is the specific heat capacity of the object ($\text{J}/\text{kg} \cdot \text{K}$), and t is the time (in seconds, s).

The convective heat transfer coefficient from an object to a cooling fluid can be determined using the Nusselt number (Nu_L) correlation, as described in Eq. (2)–(3).

$$\text{Nu}_L = \frac{hL}{k_f} \quad (2)$$

$$\text{Nu}_L = a \text{Re}^b \text{Pr}^c \quad (3)$$

In Eq. (2)–(3), L is the characteristic length (typically defined as $L \equiv V/A_s$), representing a characteristic dimension for the heat transfer process. k_f is the thermal conductivity of the fluid ($\text{W}/\text{m} \cdot \text{K}$), Nu_L is the Nusselt number, Re is the Reynolds number, Pr is the Prandtl number, and a , b , c are empirical constants used in the Nusselt number correlation equation.

The Reynolds number can be determined based on the properties of the cooling fluid and its flow velocity, as expressed in Eq. (4).

$$\text{Re} = \frac{\rho v D}{\mu} \quad (4)$$

In Eq. (4) v is the velocity of the fluid (m/s), D is the hydraulic diameter (m), and μ is the dynamic viscosity of the fluid ($\text{Pa} \cdot \text{s}$).

The Prandtl number can be determined based on the thermal properties of the cooling fluid, as expressed in Equation

$$Pr = \frac{\nu}{\alpha} = \frac{c_p \mu}{k_f} \tag{5}$$

Where ν is the momentum diffusivity (kinematic viscosity, m^2/s), α is the thermal diffusivity (m^2/s), and C_p is the specific heat capacity ($J/kg \cdot K$).

2.2 Computational Fluid Dynamics Analysis

The CFD (Computational Fluid Dynamics) simulation using Ansys Fluent is employed to model and analyze fluid flow and heat transfer within the chamber and the cooling fluid system. The steps involved in the CFD simulation of this system are as follows:

Geometry Model and Domain Creation

The geometry of the chamber and the cooling system is created in a three-dimensional design, as shown in Figure 1. In this design, solid walls are modeled in 2D (surface) and will be simulated using the shell conduction method to reduce computational time.

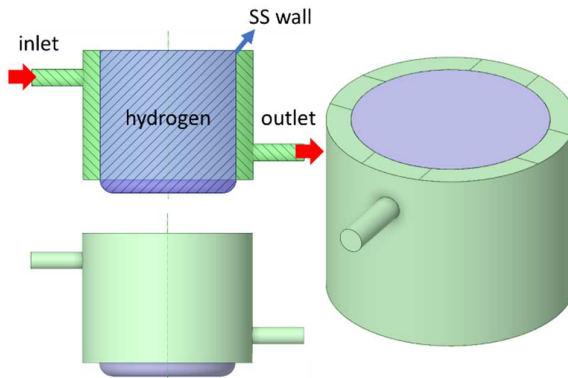


Fig. 1. Geometry of the chamber and cooling circuit domain in the CFD simulation.

Grid Generation (Meshing)

In this step, the domain is divided into discrete elements called grids or mesh. These grids form the points at which the partial differential equations for fluid flow and heat transfer will be solved. The result of grid generation can be seen in Figure 2.

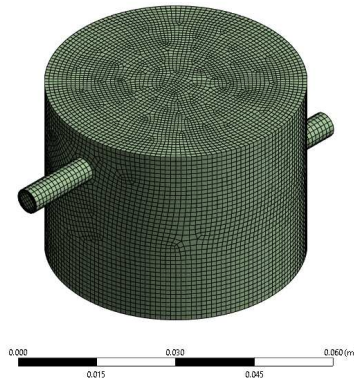


Fig. 2. Grid division of the chamber and cooling circuit in the CFD simulation.

Physical Model and Parameters

The continuity, momentum, and energy conservation equations in Ansys Fluent can be written as in Equations (42) to (44).

$$\frac{\partial \rho}{\partial t} + \nabla \cdot (\rho v) = 0 \quad (6)$$

$$\frac{\partial}{\partial t} (\rho v) + \nabla \cdot (\rho v v) = \nabla \cdot p + \nabla \cdot (\tau) \quad (7)$$

$$\frac{\partial}{\partial t} (\rho E) + \nabla \cdot (v(\rho E + p)) = \nabla \cdot (k_{eff} \nabla T + (\tau \cdot v)) \quad (8)$$

In this simulation, the k-omega SST method is used to solve the turbulence equations with constant thermophysical properties.

Boundary Condition and Simulation Strategies

The boundary conditions used in this simulation include a mass flow rate of 50 g/s at the inlet with an inlet temperature of -5 °C. The initial conditions in the hydrogen chamber are at a pressure of 20 MPa and a temperature of 200 °C. The initial wall temperature of the chamber is also set to 200 °C. The simulation process uses the SIMPLE solver in transient mode with a time step of 1 second and a total of 1800 time steps, resulting in a total transient time of 1800 seconds.

3 RESULTS AND DISCUSSIONS

3.1 Lumped Capacitance Calculation Results

Figure 3 provides a visual representation of the influence of different mass flow rates on the cooling time within the system. This data is instrumental in understanding the critical role that mass flow rate plays in the efficiency of the cooling process.

Upon examination of Figure 3, a striking pattern emerges. As the mass flow rate is escalated from 0.01 kg/s to 0.25 kg/s, there is a marked reduction in the cooling time required, plummeting from 3250 seconds to a mere 250 seconds. This significant decrease in cooling time is a direct consequence of the higher mass flow rate, which facilitates more efficient heat transfer and, in turn, leads to quicker temperature reduction within the system.

However, the figure also reveals an intriguing aspect of this relationship. Once the mass flow rate surpasses the threshold of 0.25 kg/s, further increases do not result in a substantial reduction in cooling time. In essence, the benefits of a higher mass flow rate start to plateau, indicating diminishing returns regarding cooling time reduction. This phenomenon is aptly exemplified when considering a mass flow rate of 0.4 kg/s, which results in a reduction of the required cooling time to only 200 seconds. While there is a reduction, it is not as substantial as observed when transitioning from lower flow rates to the 0.25 kg/s threshold.

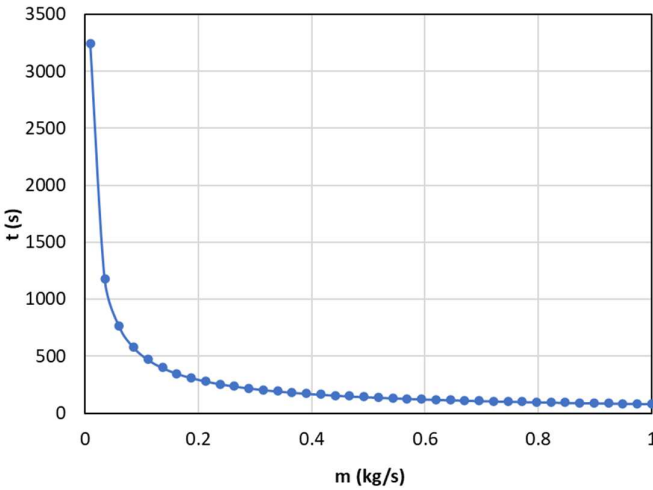


Fig. 3. Effect of mass flow rate on cooling time

This intriguing trend underscores the significance of optimizing the mass flow rate within the system. While higher flow rates indeed expedite the cooling process, there comes a point where the additional benefits in terms of reduced cooling time become less pronounced. Considering the lumped capacitance method used for these calculations, it's important to acknowledge that this method simplifies the analysis and makes various assumptions to model the heat transfer process. To ensure the accuracy of the results, it is advisable to compare the outcomes obtained through the lumped capacitance method with either more detailed analytical calculations or numerical methods like Computational Fluid Dynamics (CFD). This comparative analysis can offer a comprehensive perspective on the cooling process, helping to validate and refine the results, particularly when dealing with complex heat transfer scenarios.

3.2 CFD Simulation Results

The results obtained from the lumped capacitance method need to be validated by comparing them with the results from CFD simulations. Figure 4 displays the comparison between the lumped capacitance method and CFD simulation results. It can be seen that the calculations using the lumped capacitance method differ significantly from the CFD simulation results. This is partly due to the simplification of the heat transfer process in the lumped capacitance method, which only accounts for the heat transfer from the chamber to the cooling fluid. In contrast, CFD simulations consider heat transfer from the chamber to the ambient air through natural convection. The cooling time needed to reach the target temperature is achieved by 380 s when it is calculated using numerical approach using CFD and is achieved by 900 s when it is calculated using analytical approach of lumped capacitance method. The deviation appeared in this result is due to the simplification approach in the lumped capacitance method.

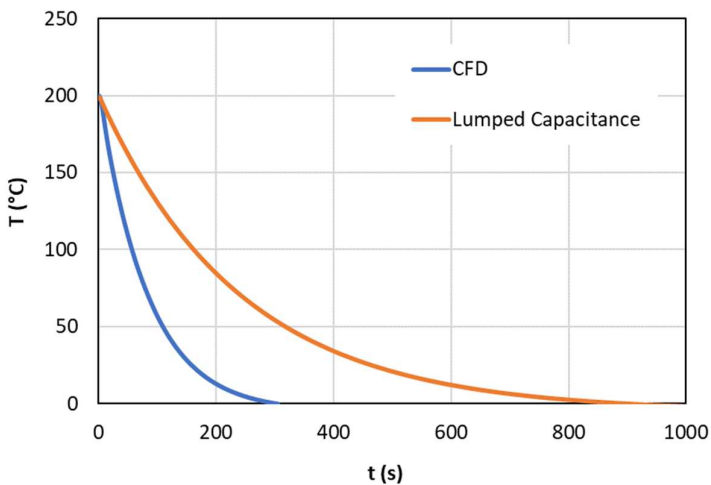


Fig. 4. The transient temperature of the object calculated using lumped capacitance and CFD

Figure 5 illustrates the change in the heat transfer rate from the chamber to the cooling fluid. From this figure, it can be observed that at the beginning of the cooling process, the heat transfer rate increases drastically to reach 700 Watts due to the high temperature difference between the chamber and the cooling fluid. Afterward, as the chamber temperature slowly decreases, the heat transfer rate from the chamber to the cooling fluid also decreases. This graph suggests that with a maximum heat transfer rate of 700 W, the thermostatic cooling bath in the Sievert apparatus installation needs to have a cooling capacity of approximately 700 W.

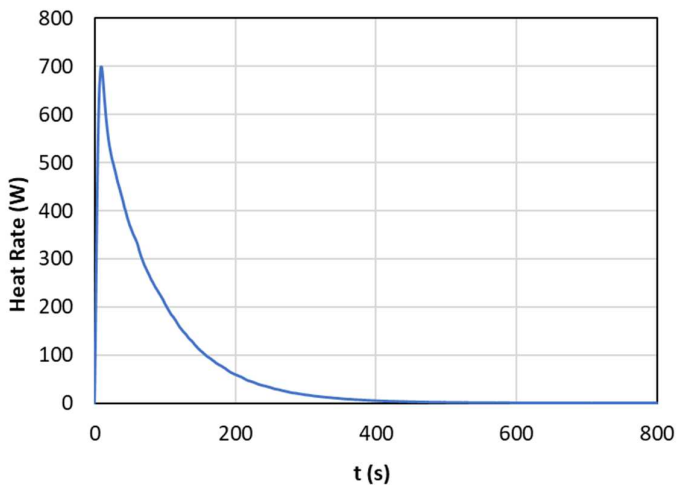


Fig. 5. The heat transfer rate during cooling process

Figure 6 provides a depiction of the distribution and temperature fluctuations within the apparatus at distinct time intervals: 100 seconds, 200 seconds, 300 seconds, and 400 seconds. These observations yield valuable insights into the thermal dynamics of the system. At the 100-second mark, the figure demonstrates a notable decrease in chamber temperature. This initial reduction is a result of the cooling process, which efficiently removes heat from the chamber, leading to a more favorable temperature profile. As time progresses, at the 200-second point, the chamber temperature continues to gradually decline. By the time 400 seconds elapse, the chamber temperature becomes remarkably uniform, indicating that the cooling process has been effectively controlled and that thermal equilibrium is approaching.

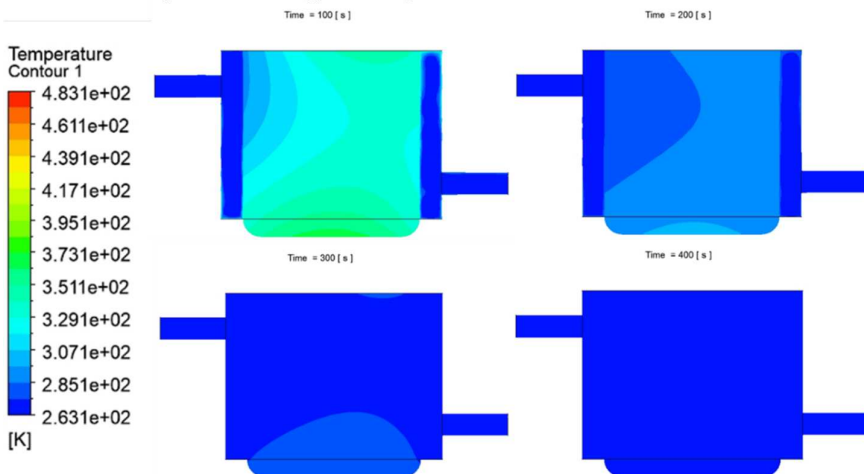


Fig. 6. The temperature distribution during cooling process

Figure 6 also highlights a critical aspect of the heat transfer mechanism within the apparatus. The area experiencing the most substantial heat transfer is situated on the inlet side, specifically the top left corner. This is evident in the lower temperature of the hydrogen within this region, a clear indicator of enhanced cooling efficiency. The cooling fluid retains a lower temperature in this specific zone compared to the other areas, fostering more efficient heat transfer and promoting quicker temperature reduction.

Conversely, the upper and lower walls of the apparatus exhibit a somewhat delayed cooling process. Notably, the lower wall experiences a more extended cooling duration. This phenomenon can be attributed to the absence of direct interaction with the cooling fluid in this region. Here, the cooling process is predominantly governed by natural convection interactions with the surrounding environment. As a result, the cooling process on the lower wall extends over a more protracted period, emphasizing the significance of the spatial relationship between the cooling fluid inlet zone and specific sections of the apparatus.

4 CONCLUSION

This paper addresses the analysis of heat transfer in the cooling process during hydrogen adsorption on carbon-based Solid State Hydrogen Storage (SSHS). The study employs two distinct methods: an analytical approach using the lumped capacitance method and a numerical method using Computational Fluid Dynamics (CFD). The central aim of this investigation is to advance our comprehension of heat transfer dynamics in the cooling phase of hydrogen adsorption on SSHS with a carbon-based structure.

The results reveal that an increase in mass flow rate from 0.01 kg/s to 0.25 kg/s leads to a significant reduction in cooling time, decreasing it from 3250 seconds to 250 seconds. However, elevating the mass flow rate beyond 0.25 kg/s does not produce a substantial further reduction in cooling time. In addition, The significant discrepancies between lumped capacitance method calculations and CFD simulations are attributed to the simplified heat transfer model of the former, which only considers heat transfer from the chamber to the cooling fluid. The maximum heat transfer rate attains 700 W and achieving the desired temperature with a coolant flow rate of 50 g/s takes only 380 seconds when employing a numerical approach through CFD, which is notably faster than the results obtained through the analytical method using lumped capacitance.

In the CFD results, the chamber's temperature experiences a significant reduction up to 200 seconds and subsequently decreases gradually until, at the 400-second mark, the chamber's temperature achieves a greater degree of uniformity. The most substantial heat transfer takes place on the inlet side, particularly at the top left, as evidenced by the reduction in hydrogen temperature in this region, since the cooling fluid maintains a lower temperature in this zone in comparison to other areas.

REFERENCES

1. H. M. Ariyadi et al., 'Flow characteristics and noise diagnosis of hydrogen charging solenoid valve in hydrogen- fueled automobile', in ECOS 2020 - Proceedings of the 33rd International Conference on Efficiency, Cost, Optimization, Simulation and Environmental Impact of Energy Systems, 2020. Author, F., Author, S.: Title of a proceedings paper. In: Editor, F., Editor, S. (eds.) CONFERENCE 2016, LNCS, vol. 9999, pp. 1–13. Springer, Heidelberg (2016)
2. H. M. Ariyadi, J. Jeong, and K. Saito, 'Computational analysis of hydrogen flow and aerodynamic noise emission in a solenoid valve during fast-charging to fuel cell automobiles', *J Energy Storage*, vol. 45, p. 103661, Jan. 2022, doi: 10.1016/j.est.2021.103661.
3. D. Rahmalina, R. A. Rahman, A. Suwandi, and Ismail, 'The recent development on MgH₂ system by 16 wt% nickel addition and particle size reduction through ball milling: A noticeable hydrogen capacity up to 5 wt% at low temperature and pressure', *Int J Hydrogen Energy*, vol. 45, no. 53, pp. 29046–29058, Oct. 2020, doi: 10.1016/j.ijhydene.2020.07.209.
4. United States Department of Energy, 'Target Explanation Document: Onboard Hydrogen Storage for Light-Duty Fuel Cell Vehicles', Washington, D.C. Accessed: Oct. 16, 2023. [Online]. Available: <https://www.energy.gov/eere/fuelcells/downloads/target-explanation-document-onboard-hydrogen-storage-light-duty-fuel-cell>
5. J. Zhang, S. Yan, and H. Qu, 'Recent progress in magnesium hydride modified through catalysis and nanoconfinement', *Int J Hydrogen Energy*, vol. 43, no. 3, pp. 1545–1565, Jan. 2018, doi: 10.1016/j.ijhydene.2017.11.135.
6. W. XU *et al.*, 'Investigation of hydrogen storage capacity of various carbon materials', *Int J Hydrogen Energy*, vol. 32, no. 13, pp. 2504–2512, Sep. 2007, doi: 10.1016/j.ijhydene.2006.11.012.
7. I. for E. and T. B. D. Joint Research Centre, Hydrogen sorption measurements on potential storage materials experimental methods and measurement accuracy. Publications Office, 2008.
8. X. Yu, J. Li, Z. Chen, K. Wu, L. Zhang, and S. Yang, 'Effects of helium adsorption in carbon nanopores on apparent void volumes and excess methane adsorption isotherms', *Fuel*, vol. 270, 2020, doi: 10.1016/j.fuel.2020.117499.
9. D. BROOM, 'The accuracy of hydrogen sorption measurements on potential storage materials', *Int J Hydrogen Energy*, vol. 32, no. 18, pp. 4871–4888, Dec. 2007, doi: 10.1016/j.ijhydene.2007.07.056.
10. K. S. W. Sing, 'Reporting physisorption data for gas/solid systems with special reference to the determination of surface area and porosity (Recommendations 1984)', *Pure and Applied Chemistry*, vol. 57, no. 4, pp. 603–619, Jan. 1985, doi: 10.1351/pac19857040603.

Open Access This chapter is licensed under the terms of the Creative Commons Attribution-NonCommercial 4.0 International License (<http://creativecommons.org/licenses/by-nc/4.0/>), which permits any noncommercial use, sharing, adaptation, distribution and reproduction in any medium or format, as long as you give appropriate credit to the original author(s) and the source, provide a link to the Creative Commons license and indicate if changes were made.

The images or other third party material in this chapter are included in the chapter's Creative Commons license, unless indicated otherwise in a credit line to the material. If material is not included in the chapter's Creative Commons license and your intended use is not permitted by statutory regulation or exceeds the permitted use, you will need to obtain permission directly from the copyright holder.

